


## Hole Self-Trapping in $\text{Y}_3\text{Al}_5\text{O}_{12}$ and $\text{Lu}_3\text{Al}_5\text{O}_{12}$ Garnet Crystals

V. Laguta,\* M. Buryi, J. Pejchal, V. Babin, and M. Nikl

*Institute of Physics AS CR, Cukrovarnicka 10, 16253 Prague 6, Czech Republic*

 (Received 4 December 2017; revised manuscript received 10 March 2018; published 26 September 2018)

The processes of hole localization in  $\text{Y}_3\text{Al}_5\text{O}_{12}$  and  $\text{Lu}_3\text{Al}_5\text{O}_{12}$  single crystals are investigated by electron paramagnetic resonance (EPR) and thermally stimulated luminescence (TSL). It is found that holes created by x-ray irradiation at 77 K are predominantly self-trapped at regular oxygen ions forming an  $\text{O}^-$  hole center. This self-trapped hole (STH) center is thermally stable to about 100 K in both yttrium aluminum garnet  $\text{Y}_3\text{Al}_5\text{O}_{12}$  (YAG) and lutetium  $\text{Lu}_3\text{Al}_5\text{O}_{12}$  garnet (LuAG) crystals. At higher temperatures, thermally liberated holes are retrapped at oxygen ions in the vicinity of an acceptor ion such as  $\text{Mg}^{2+}$  and  $\text{Al}_Y$  or  $\text{Al}_{Lu}$  antisite ions which leads to an increase in the thermal stability of the trapped hole approximately equal to 150 K. TSL measurements show two composite glow peaks in the temperature range of 77–280 K, the temperature positions of which correlate well with the thermal stability of the  $\text{O}^-$  centers. The hole thermal ionization energy is determined from a numerical fit of the TSL peaks within the model of second-order kinetics. It is in the range of 0.25–0.26 eV for an  $\text{O}^-$  STH center, and increases to 0.41–0.45 eV for an  $\text{O}^-$  center stabilized by the acceptor. Revealed  $\text{O}^-$  centers can be attributed to  $\text{O}^-$  small polarons formed mainly due to hole stabilization by short-range interactions with the surrounding lattice. Knowledge of the nature of color centers and related trapping sites is critically important for further optimization of all garnet scintillation materials.

DOI: [10.1103/PhysRevApplied.10.034058](https://doi.org/10.1103/PhysRevApplied.10.034058)

### I. INTRODUCTION

Among many scintillating single crystals, yttrium aluminum garnet  $\text{Y}_3\text{Al}_5\text{O}_{12}$  (YAG) [1–3] and especially lutetium  $\text{Lu}_3\text{Al}_5\text{O}_{12}$  garnet (LuAG) doped by luminescent  $\text{Ce}^{3+}$  or  $\text{Pr}^{3+}$  ions are known as very efficient scintillators due to high density (LuAG), good light yield, and mechanical and chemical resistance [4–7]. YAG:Ce became widely used a long time ago for the detection of electron beams, e.g., in scanning electron microscopy [2] and as a blue-to-yellow downconverter phosphor in white light emitting diodes [8]. Both LuAG:Ce and YAG:Ce have also recently gained attention for high energy physics applications due to exceptionally high radiation resistance [9], which could enable their use, e.g., in the fiber form [10] in future calorimetric or dual read-out detectors in this field. These crystals are usually grown from melt by the Czochralski [11,12] or Bridgman [13] techniques. In spite of the favorable scintillation properties, their main disadvantage is the presence of slow components in the scintillation decay [14], which appears due to delayed radiative recombination at  $\text{Ce}^{3+}$  ions. This phenomenon causes serious degradation of the light yield and timing characteristics as more than 50% of the light yield is released in these slower decay components which are undoubtedly related to the host traps [14–16]. The origin of such traps in many

cases can be clarified by electron paramagnetic resonance (EPR) study, especially when the EPR measurements are correlated with corresponding thermally stimulated luminescence (TSL) data [5,17].

During the last several years, systematic efforts have been devoted to further improve the time characteristics of the garnet-based scintillators by an admixture of gallium and gadolinium [18–25], the effect of which was explained by the removal of shallow electron traps due to the shift of the conduction band edge to lower energies [26]. By composition engineering (tailoring), a new family of materials, so-called multicomponent garnet scintillators, has been further developed. The balanced admixture of Ga and Gd into YAG and LuAG, with the general chemical formula  $(\text{Gd}, \text{Lu}, \text{Y})_3(\text{Ga}, \text{Al})_5\text{O}_{12}:\text{Ce}$  resulted in a suppressed trapping effect and enormously increased the light yield above 50 000 ph/MeV [27]. Such value considerably exceeds those achieved for the best Ce-doped orthosilicate scintillators.

The lattice defects (or color centers) which cause change or modification of the optical and scintillation properties of the YAG and LuAG crystals have been previously studied in many publications (see, for instance, review papers [5,28,29]). Among different possible defects, so-called antisite ion defects, i.e., Y or Lu at the Al site and vice versa and oxygen vacancies are the most frequently mentioned intrinsic defects in garnet crystals [30–33]. They serve as electron traps [34]. However, it should be

\*laguta@fzu.cz

emphasized that while the  $Y_{Al}$  antisite ions were directly detected by NMR and electron traps based on the antisite defect were identified by EPR methods in  $YAlO_3$  crystals [35,36], no antisite ions were found in  $^{27}Al$  and  $^{89}Y$  NMR spectra of YAG and LuAG [37–40] suggesting that the concentration of such defects is, in fact, much lower than that in  $YAlO_3$ . On the other hand, oxygen vacancies and related traps, for instance,  $F^+$  centers in YAG/LuAG, were documented by EPR [41] and even by electron-nuclear double resonance technique [42].

Although the influence of the antisite and oxygen vacancy-related traps on delayed recombination of carriers in YAG/LuAG can be effectively diminished by Ga codoping (it lowers the conduction-band edge and thus removes the electron trapping effect), similar band gap “engineering” for hole traps suggested by theoretical calculations [26] has not yet been technologically realized. Therefore, identification and further detailed investigation of the hole traps in garnet crystals is of crucial importance for pushing the performance of these materials close to the intrinsic limits. This aspect is particularly important with the introduction of divalent codoping in garnet scintillators which, apart from the positive effect due to stabilization of the  $Ce^{4+}$  center, can introduce hole centers in the anion oxygen sublattice to recover charge balance in the structure [43,44] and such centers might negatively influence the scintillation mechanism. The light-yield value of the best quality YAG:Ce and LuAG:Ce single crystals or ceramics commercially available is around 30 000 photons/MeV [7,28,45], which is about half of the theoretically predicted value [46]. This means there is room for further material improvement.

It is well known that the most common hole-type defect always present in oxide materials is  $O^-$  ion, i.e., a hole trapped at the oxygen lattice ion [35,47–50]. Such a defect can usually be created by a hole self-trapping, but further stabilization of a hole at the oxygen ion can be provided by another defect nearby, ensuing the thermal stability of the hole center in the temperature range from about 20–30 K up to room temperature. Of course, the number of created  $O^-$  ions depends on many factors but, in general, self-trapping is a quite effective mechanism of charge-carrier trapping. Because the  $O^-$  ion is paramagnetic (electronic configuration  $2p^5$ , electronic spin  $S = 1/2$ ), it can be, in principle, easily detected and subsequently studied in detail by EPR. The thermal release of holes from  $O^-$  ions also leads to the intense TSL peaks reported for many materials [17,35,48–50].

In spite of the great importance of the  $O^-$  centers in garnet crystals, there are only a few publications devoted to EPR of these centers. The first observation of an EPR spectral line which could be assigned to  $O^-$  ions in YAG was mentioned in [41]. However, the most detailed previous study was performed on LuAG ceramics doped with Ce and Mg ions [43]. Some preliminary data were also

reported for LuAG crystals doped with Pr and Mg ions [15,51]. In all these publications, a hole-type paramagnetic center was identified in EPR spectra created by x-ray [15,51] or light [43] irradiation of samples at 77 K. The g factor of this hole center as well as density functional theory (DFT) modeling [43] suggested that it could be  $O^-$  ion, i.e., a hole trapped at the  $O^{2-}$  lattice ion, presumably in the vicinity of the Mg impurity ion. While this interpretation seems to be quite correct, no valid experimental arguments have yet been presented to clarify the nature and actual structure of this center as well as to show a clear correlation of its thermal stability with TSL peaks.

In the present paper, we report results of comprehensive EPR investigation of  $O^-$  centers in both YAG and LuAG crystals either nominally pure or doped by  $Mg^{2+}$  ions. The EPR data are compared with TSL data obtained for the same crystals. Our results suggest that the holes generated by irradiation at cryogenic temperatures ( $T < 100$  K) in garnet crystals are predominantly self-trapped at oxygen lattice ions in the form of  $O^-$  centers. The paper is organized in the following way: After a short description of the applied experimental methods (Sec. II), we first report our EPR data on an  $O^-$  center created by x-ray irradiation at 77 K and show that this center is formed by a hole self-trapping (Sec. III A). Then we present data on the  $O^-$  perturbed center (Sec. III B). Section III C reports the thermal stability of  $O^-$  centers and their correlation with TSL. Finally, in Sec. IV, we draw conclusions.

## II. EXPERIMENTAL DETAILS

The YAG and LuAG crystals are grown by the micro-pulling-down method with rf inductive heating [52]. An iridium crucible with a die of 3 mm in diameter is used. The growth is performed under a  $N_2$  atmosphere using a  $\langle 111 \rangle$  and  $\langle 100 \rangle$  oriented YAG or LuAG single crystal as a seed. The starting materials are prepared by mixing 4N purity  $Y_2O_3$  or  $Lu_2O_3$  and  $Al_2O_3$  powders.  $MgCO_3$  of 4N purity is added to the mixture for the Mg-codoped samples. The concentration of Mg impurity is varied from 100 up to 3000 atomic ppm. The crystals are in the form of rods with diameters of 3 mm and lengths of 2–3 cm.

The EPR spectra are measured using the commercial Bruker X/Q-band E580 ELEXSYS spectrometer at X-band (microwave frequency 9.25–9.5 GHz) within the temperature range 10–290 K. An x-ray tube operating at a voltage and current of 55 kV and 30 mA, respectively, with a Co anode (ISO-DEBYEFLEX 3003 Seifert GmbH.) was used as a source of x-ray irradiation of crystals at the liquid nitrogen (LN) temperature.

The same x-ray irradiation source is used for TSL excitation. The Optistat cryostat, Oxford Instruments, is used to control the sample temperature. After irradiation at 77 K, the TSL run is initiated with a heating rate of 6 K/min. The TSL signal is recorded using two registration channels:

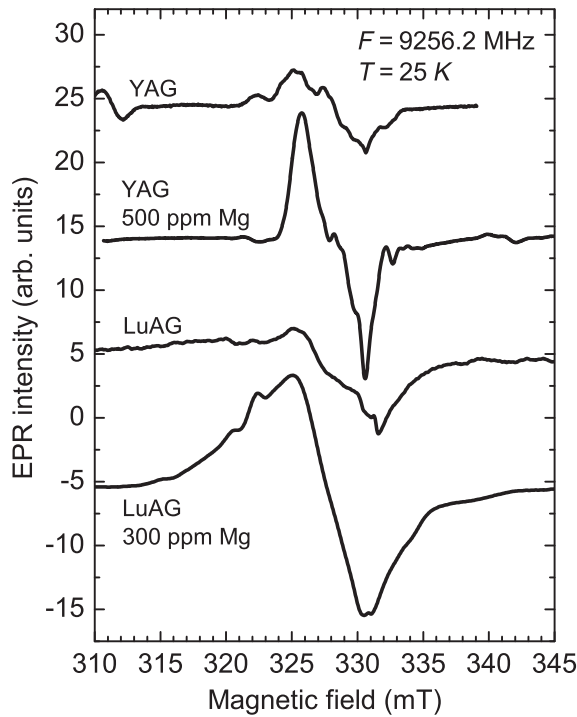


FIG. 1. EPR spectra in YAG and LuAG crystals created by x-ray irradiation at 77 K. The crystals have arbitrary orientations.

(i) spectrally unresolved, by TBX detector downstream the monochromator, which was set to zero order in spectrofluorimeter TEMPRO, Horiba Jobin Yvon, with a sampling rate of 1 s; (ii) spectrally resolved, by cooled CCD detector in the Ocean Optics spectrometer. In this case, the spectra within 200–800 nm are taken every 10 s. For all measurements, the TSL is monitored within 77–500 K.

### III. EXPERIMENTAL RESULTS

#### A. Self-trapped hole center

Before x-ray irradiation, all samples show EPR spectra of the  $\text{Fe}^{3+}$  and  $\text{Yb}^{3+}$  ions always present in YAG and LuAG crystals as accidental impurities [53,54]. After x-ray irradiation at the LN temperature of  $T = 77$  K, a new spectrum arises which we further later attribute to an  $\text{O}^-$  ion. It consists of a single broad line without a distinctively resolved structure (Fig. 1).

Because the intensity of the  $\text{O}^-$  spectrum markedly increases if the crystal is doped by  $\text{Mg}^{2+}$  ions, qualitative analysis of the spectra is mainly performed in Mg-doped crystals.

The spectral line, which in LuAG crystals is much broader than that in YAG, is completely isotropic, i.e., it conserves both the shape and resonance field under crystal rotation with respect to the magnetic field direction. In contrast to LuAG, the spectral line in YAG, which is narrower, clearly changes its shape under crystal rotation

(Fig. 2, left panel) conserving, however, the center of gravity. The specific line shape with sharp edges suggests that it originates from an unresolved hyperfine (HF) structure. This is confirmed by simulation of the spectra by introducing the HF interaction of electron spin with two Al nuclei having nuclear spins of  $5/2$  and 100% natural abundance. All major variations in the spectral line shape are obtained by changing HF constant values for two Al nuclei. As an example, the simulated spectrum is shown in Fig. 2, left panel for two crystal orientations (solid blue lines). The simulation is done with the following spin Hamiltonian:

$$H = g\beta SB + I_1 A_1 S + I_2 A_2 S, \quad (1)$$

where  $g = 2.020$  is the  $g$  factor,  $S = 1/2$  is the electron spin,  $\beta$  is the Bohr magneton,  $B$  is the magnetic field, and  $I_1$  ( $I_2$ ) and  $A_1$  ( $A_2$ ) are the  $^{27}\text{Al}$  nuclear spins and HF constants, respectively. Depending on the crystal orientation, the  $^{27}\text{Al}$  HF splitting is in the range of  $(3\text{--}7.7) \times 10^{-4} \text{ cm}^{-1}$ .

Both the positive  $g$  factor shift with respect to the free electron value and the presence of two Al ions in the vicinity of the paramagnetic particle indicate that the EPR spectrum belongs to a hole center created by localization of a hole at oxygen in the form of an  $\text{O}^-$  ion. Namely, oxygen sites in the garnet structure have two adjacent Al ions at the distances 1.761 and 1.937 Å (YAG) and 1.760 and 1.939 Å (LuAG) [55] as is seen from the fragment of the LuAG (YAG) structure with a model of the  $\text{O}^-$  center (Fig. 2, right panel). These two Al ions belong to an oxygen tetrahedron ( $\text{Al}^{\text{tet}}$ ) and an oxygen octahedron ( $\text{Al}^{\text{oct}}$ ).

Of course, the  $\text{O}^-$  center has several magnetically inequivalent positions in the lattice allowed by the  $Ia\bar{3}d(230)$  space group and should also show an anisotropy of the  $g$  factor. However, all these features are masked by strong HF interactions, which are even stronger in LuAG, leading to a smooth Gaussian line shape due to additional HF interaction with nuclear spins of two adjacent Lu ions,  $\text{Lu}^{\text{dod}}$  in Fig. 2.  $^{175}\text{Lu}$  isotope has a nuclear spin of  $7/2$ , natural abundance of 97.4%, and large nuclear magnetic and quadrupole moments [56]. Therefore, the spectral line in LuAG is expected to be much broader compared to that of YAG where the  $^{89}\text{Y}$  isotope has a nuclear spin of only  $1/2$  and a more than two times smaller Larmor frequency.

The  $\text{O}^-$  center in both YAG and LuAG is thermally stable to only approximately 100 K. Its thermal stability is determined by the pulse annealing method. After irradiation at 77 K, the sample is quickly cooled down to 20–30 K and then is heated at a rate of 0.5–1 K/s up to a certain temperature  $T_{\text{an}}$ , held at that temperature for 3–4 min, and then quickly cooled down (with a rate of 1–2 K/s) to a fixed temperature where the center is thermally stable and the EPR intensity can easily be measured. Dependence of the  $\text{O}^-$  EPR spectrum on the pulse annealing temperature is shown in Figs. 3(a) and 3(b) for YAG and LuAG, respectively. In

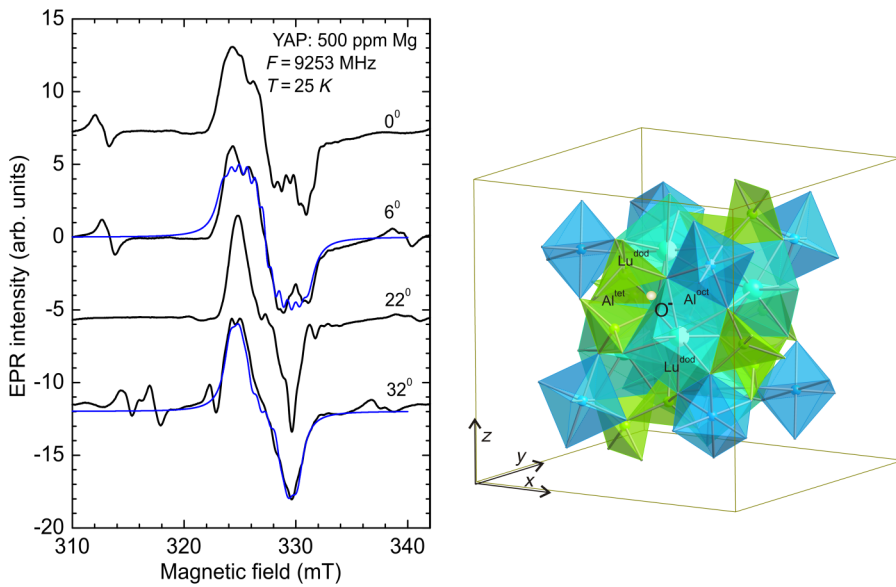


FIG. 2. Left panel: angle variation of the  $O^-$  EPR spectrum in YAG: 500 ppm Mg crystal and its simulation (blue solid lines). The right panel shows a fragment of the LuAG (YAG) crystal structure with an  $O^-$  ion which is shared by the Al tetrahedron (green color), Al octahedron (blue color), and two Lu(Y) dodecahedrons (light blue color).

both crystals, the intensity of the EPR spectrum decays if the crystal is heated to  $T > 100$  K and the spectrum completely disappears at annealing to 130–150 K. The same thermal stability of the  $O^-$  center is also obtained in Mg-doped crystals where, however, a new spectrum arises after annealing to 130–150 K (see next Secs. III B and III C). We assign the  $O^-$  spectrum created by x-ray irradiation at 77 K to the self-trapped hole (STH) at the  $O^{2-}$  ion since this ion is not visibly perturbed by other defects and its spectrum is present in both YAG and LuAG independently of the impurity content in the crystals (see also Fig. 1). The fact that  $Mg^{2+}$  doping essentially increases the concentration of these  $O^-$  hole centers also supports the model of this center because  $Mg^{2+}$  substituting for  $Y^{3+}$  or  $Lu^{3+}$  acts

as an acceptor. It is worth noting that the  $O^-$  STH center was already identified in many oxide crystals, including  $YAlO_3$ , see e.g., [35], however, it has not been yet reported for garnet crystals.

### B. $O^-$ perturbed center

When crystals doped by acceptor  $Mg^{2+}$  ions are annealed to 130–150 K, instead of the STH spectrum, a new spectrum arises [Fig. 4(a)]. The spectrum is very visible in YAG, but due to the broad line width, a barely perceptible difference is seen between two spectra in LuAG [Fig. 4(b)]. This new spectrum has a smaller  $g$  factor shift ( $g = 2.014$ – $2.015$ ) as compared to the STH spectrum and is

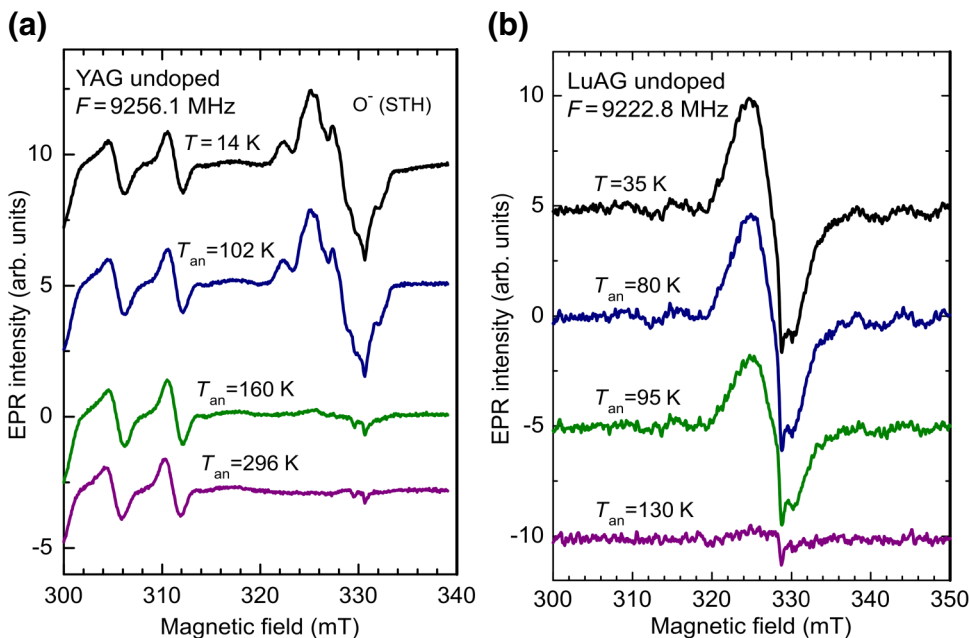


FIG. 3. Dependence of the  $O^-$  EPR spectrum in YAG (a) and LuAG (b) on pulse annealing. X-ray irradiated crystals are heated to a given annealing temperature  $T_{an}$ , held at that temperature for 3–4 min, and then cooled down to the fixed temperature of 14 K (YAG) or 35 K (LuAG) where the EPR spectrum is measured for all annealing temperatures.



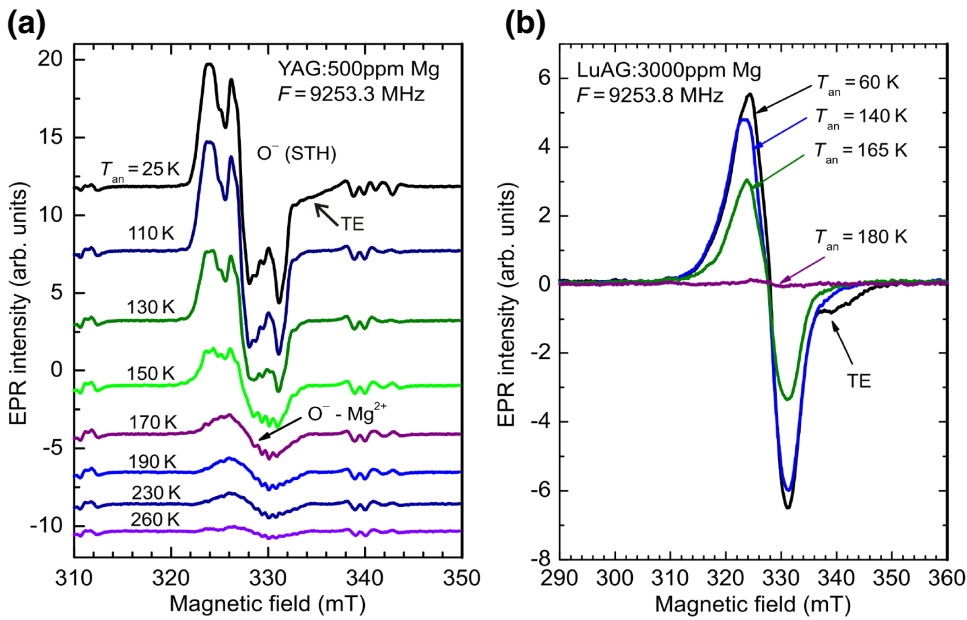


FIG. 4. Dependence of the  $O^-$  EPR spectrum in YAG (a) and LuAG (b) on pulsed annealing showing the transformation of the  $O^-$  STH spectrum into the spectrum of an  $O^-$  ion perturbed by a nearby defect. The shoulder at the right side of the  $O^-$  spectral line (indicated as TE) originates from the trapped electron center.

thermally stable to about 160 K. We attribute this spectrum to a hole trapped at an  $O^{2-}$  ion perturbed by a defect, most probably a  $Mg^{2+}$  impurity ion, since its appearance clearly correlates with the Mg doping.

Note that EPR spectrum of x-ray irradiated Mg-doped crystals also contains a shoulder at the right side of the spectral line (labeled as a trapped electron (TE), in Fig. 4) at the magnetic field corresponding to an electron-type paramagnetic particle ( $g = 1.98$ ,  $g$  factor shift is negative). We can thus assume that this signal originates from the trapped electron center, for instance,  $Lu_{Al}$  and  $Y_{Al}$  antisite ion which has trapped an electron. The shoulder in the spectrum disappears at almost the same temperature as that when holes start to liberate from the STH centers, indicating that part of the liberated holes recombines at the TE center. Alternatively, the signal at  $g = 1.98$  can be ascribed to a  $F^+$  center, i.e., an electron trapped at an oxygen vacancy. But, even in this case, the trapped electron will be delocalized over neighboring cations. The  $g$  factor

shift will mainly be determined by a contribution from  $d^1$  orbitals of the Lu or Y ions similar to, for instance, the  $F^+$  center in YAP [17,35] and  $Y_2SiO_5$  [49].

In YAG:Mg crystals, the spectrum of an  $O^-$  perturbed ion shows a partly resolved HF structure, illustrated in Fig. 5 together with the simulated HF structure.

The simulated HF structure of the  $O^-$  perturbed center is calculated using the spin Hamiltonian (1) with three HF terms:

$$H = g\beta SB + I_1 A_1 S + I_2 A_2 S + I_3 A_3 S. \quad (2)$$

The simulated parameters are:  $g = 2.015$ ;  $I_1 = I_2 = I_3 = 5/2$ ;  $A_1 = 7.3 \times 10^{-4} \text{ cm}^{-1}$ ,  $A_2 = 6.8 \times 10^{-4} \text{ cm}^{-1}$ , and  $A_3 = 6.3 \times 10^{-4} \text{ cm}^{-1}$  with each HF component having the same Gaussian line width of 0.67 mT. The fit is not ideal. However, the simulated spectrum properly describes all characteristic features of the measured one such as the number of HF components and the distribution of their

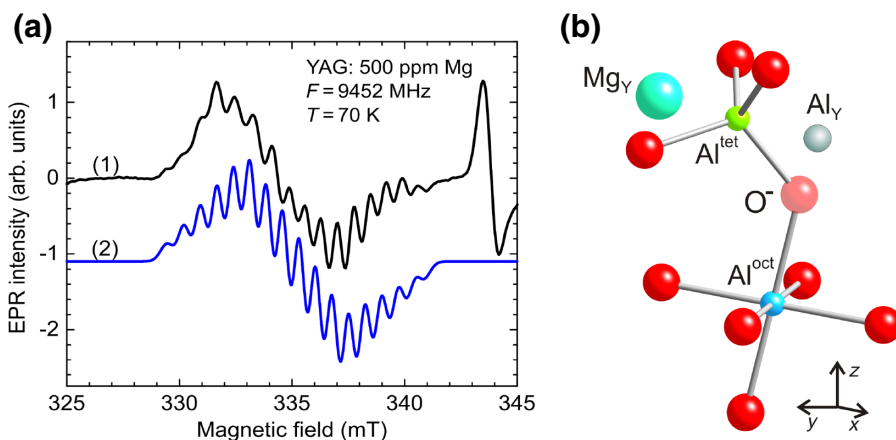


FIG. 5. (a) EPR spectrum of the  $O^-$  perturbed center (1) and its simulation (2) in YAG doped with 500 ppm Mg. (b) Model of the  $O^-$  perturbed center: it is assumed that the perturbation is due to the presence of  $Mg^{2+}$  impurity and  $Al_Y$  antisite ion.

intensities. The discrepancy between the calculated and measured spectra is related to a slight inequality of HF splitting along the HF pattern due to anisotropy of both the  $g$  factor and HF interaction. It is difficult to include this anisotropy in the calculation due to its uncertain value and the existence of several magnetically inequivalent positions of the center.

The HF parameters determined suggest the presence of a third Al ion in the vicinity of the  $O^-$  ion. In a regular garnet lattice, except for two adjacent Al ions, all other Al ions are located far from oxygen ions (the shortest next-nearest-neighbor O–Al distance is 3.297 Å). Then, the only reasonable possibility to explain the HF structure is the presence of an Al ion at the Y or Lu site, the so-called  $Al_Y$  and  $Al_{Lu}$  antisite defects, widely discussed in literature [30–34]. In this case, the above determined HF parameters are well explained as due to the interaction of a hole with the nuclear magnetic moments of three  $^{27}Al$  nuclei located at distances of 1.76, 1.94, and 2.276 Å from the oxygen ion in the unrelaxed lattice [Fig. 5(b)]. In this model of the center, we cannot be completely sure if the second closest  $Y^{3+}$  ion is substituted by a  $Mg^{2+}$  ion. Mg has one isotope with a non-zero nuclear spin  $I = 5/2$ , but it has only 10% natural abundance, which makes its contribution to the HF structure negligibly small. From a general point of view and in accordance with the DFT calculation [44], the  $O^-$ – $Mg^{2+}$  charge-compensated pair is energetically favorable. Additional stabilization of the center is provided by an  $Al_{Lu}$  or  $Al_Y$  antisite ion. However, while the antisite ion changes the spectral parameters of the  $O^-$  ion, mainly the HF interaction, its influence on the thermal stability of the trapped hole should be much weaker as compared to the  $Mg^{2+}$  acceptor ion. Such  $O^-$  centers stabilized by an acceptor are the most frequently occurring defects created under light or x-ray irradiation in oxides [47]. Note that similar  $O^-$  centers have been observed in  $YAlO_3$  [35,57]. The detailed study shows that they are attributed to small (or bound small) polarons [57]. In principle, the modern theories of polarons consider the self-trapped particle as an extreme case of small polarons (localized small polarons) [58,59], which explains the mechanism of particle localization in the lattice as due to strong electron-phonon interaction. In highly symmetric lattices, the localized electron or hole state can be additionally stabilized by the Jahn-Teller or pseudo Jahn-Teller local distortion of the lattice [60]. Such a polaron is called a Jahn-Teller small polaron. Obviously, the Jahn-Teller mechanism can be realized in YAG/LuAG lattice due to its cubic symmetry.

### C. Thermal stability of $O^-$ centers and correlation with TSL

The thermal stability of the x-ray created  $O^-$  centers is studied in detail by the pulse annealing method in YAG and LuAG crystals doped by Mg, where the EPR signal

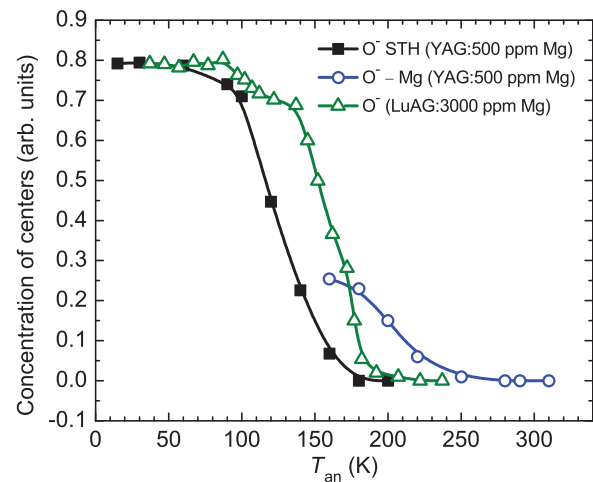


FIG. 6. Relative concentrations of  $O^-$  centers in YAG: 500 ppm Mg and LuAG: 3000 ppm Mg crystals as a function of pulse annealing temperature.

from the  $O^-$  centers is strong. The annealing temperature step is 10–20 K with an annealing time of 4 min. The 4 min interval is determined as the optimum balance between good thermalization of the sample and sufficient reproducibility of the measured EPR intensities. However, due to the limitation in the heating and cooling speeds, the actual annealing time at  $T > 200$  K is about 20–25% longer. The spectrum intensities obtained by double integration of the spectral line are recalculated in relative concentrations for  $O^-$  centers and are depicted in Fig. 6 for YAG:Mg and LuAG:Mg. It can be seen that the concentration of the  $O^-$  STH centers diminishes upon annealing to 120–130 K in YAG. Approximately at these temperatures, the  $O^-$ – $Mg^{2+}$  center appears. Its concentration decreases at  $T > 190$  K. This center completely disappears at an annealing temperature of approximately 250 K. In the case of LuAG crystals, spectral lines from the  $O^-$  STH center and  $O^-$  center stabilized by an impurity ion can hardly be separately distinguished. Therefore, experimental data for LuAG in Fig. 6 are presented as a sum of contributions from both types of centers. Nevertheless, one can see a marked decrease in the total concentration of  $O^-$  centers at the temperature where the STH centers disappear in YAG. This confirms that similar  $O^-$  STH centers exist in LuAG as well. The further sharp decrease of the  $O^-$  concentration corresponds to the thermal disintegration of the  $O^-$ – $Mg^{2+}$  centers.

In order to get a deeper insight into the kinetics of the trapped holes and to determine their thermal stability parameters, we perform TSL measurements of the crystals irradiated by x-ray at 77 K. The results are shown in Fig. 7 for the same crystals we use in the EPR measurements. The first intense TSL peak in both YAG and LuAG is detected at 118–122 K, exactly at the temperatures where

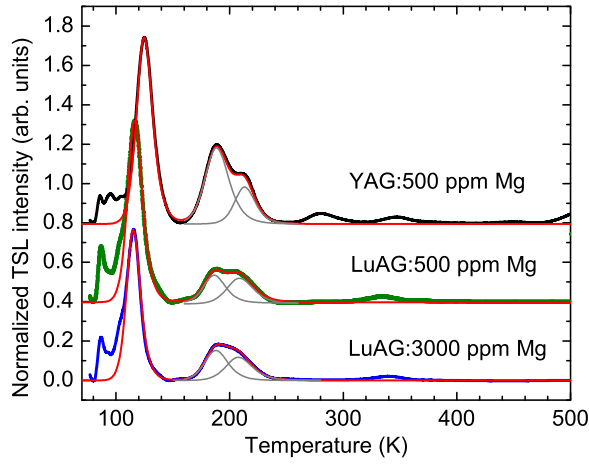


FIG. 7. Normalized TSL glow curves of YAG:500 ppm Mg, LuAG:500 ppm Mg, and LuAG:3000 ppm Mg crystals irradiated by x-rays at 77 K measured at the heating rate of 6 K/min. Red solid lines are simulated TSL peaks; gray lines represent individual peaks for the composite TSL peak at 200 K. Glow curves are vertically shifted for better visualization.

the  $O^-$  STH center undergoes thermal destruction. The second, composite TSL peak around 200 K is obviously related to the thermal disintegration of the  $O^-Mg^{2+}$  centers. The intensity of this peak substantially diminishes in undoped crystals and completely disappears in high purity crystal (see, e.g., Fig. 2 in [16]). The peaks at  $T > 280$  K may originate from the thermal release of electrons from oxygen vacancies or  $Lu_{Al}$  ( $Y_{Al}$ ) antisite defects. However, their origin needs further investigation.

The TSL glow curve numerical analysis is based on the well-known formula of Garlick-Gibson [61] valid for the second-order recombination kinetics. This kinetics leads to an almost symmetrical shape of the TSL glow curve in agreement with the experiment. The results of the TSL peaks simulation are displayed in Fig. 7 by the red and gray solid lines to the temperature 260 K. The fit is quite good taking into account the composite character of the TSL peaks. Nevertheless, in the simulation of the TSL curve, we try to use a minimum number of traps to provide only characteristic features of the observed TSL. In particular, we assume that only one trap ( $O^-$  STH center) mainly contributes to the first peak at 118–122 K. The second, composite TSL peak around 200 K is simulated assuming the presence of two traps contributing to this peak (gray lines in Fig. 7). The thermal stability parameters of the traps are listed in Table I. One can see that the peaks related to the  $O^-$  STH center are described by approximately the same parameters in all three crystals: the thermal depth is 0.252–0.264 eV and the effective frequency factor  $s'$  varies from  $4.6 \times 10^6 s^{-1} m^3$  in YAG to  $5 \times 10^7 s^{-1} m^3$  in LuAG. The second two peaks at 186–214 K have a much larger thermal depth of 0.409–0.45 eV. The complex character of

TABLE I. Thermal stability of traps visible in TSL glow peaks in YAG and LuAG crystals with Mg impurity. The error in  $E_T$  value is less than 5%, while it could be up to 25% for the effective frequency factor  $s'$ .

Crystal	$T_m$ (K)	Thermal depth $E_T$ (eV)	Frequency factor $s'$ ( $s^{-1} m^3$ )
YAG:500 ppm Mg	125	0.264	$4.6 \times 10^6$
	188	0.409	$1 \times 10^7$
	214	0.62	$1.5 \times 10^{11}$
LuAG:500 ppm Mg	116	0.252	$1 \times 10^7$
	186	0.44	$3 \times 10^8$
	209	0.45	$2 \times 10^7$
LuAG:3000 ppm Mg	116	0.262	$5 \times 10^7$
	188	0.418	$5 \times 10^7$
	208	0.446	$2 \times 10^7$

the TSL curve around 200 K with variations in shape from crystal to crystal suggests the presence of several traps of the same origin, namely originating from the  $O^-$  hole centers stabilized by a defect nearby. We also cannot exclude a more complex character of the hole excitation from the  $O^-$  ion than the simple one ascribed by the Arrhenius law. In any case, it is clear that the main contribution to TSL in Mg-doped crystals around 200 K is coming from the  $O^-Mg^{2+}$  centers, as this peak substantially diminishes in undoped pure crystals.

#### IV. CONCLUSIONS

EPR measurements are carried out in YAG and LuAG crystals irradiated by x-rays at 77 K. The crystals are both nominally pure and doped by Mg. The measurements clearly reveal  $O^-$  hole centers, which are attributed to (i) a STH at the lattice oxygen ion and (ii) a hole at the oxygen ion additionally stabilized by a perturbing defect nearby, namely, in the case of Mg doping, this defect is  $Mg^{2+}$  substituting for  $Y^{3+}$  or  $Lu^{3+}$  and  $Al_Y$  or  $Al_{Lu}$  antisite ions.

The  $O^-$  STH center is thermally stable to about 100 K in both the YAG and LuAG crystals. The  $O^-$  perturbed center ( $O^-Mg^{2+}$ ) is stable to approximately 160 K. These hole centers can be attributed to  $O^-$  small polarons. In the small polaron model, the hole localization is caused predominantly by the short-range lattice distortions. Therefore, a more appropriate approach to model such centers should be based on the DFT calculation as it was demonstrated in [43]. In particular, the trap depth of 1 eV is predicted for the Mg-perturbed  $O^-$  center in LuAG. This energy is only about two times larger than the measured one, demonstrating a quite good result as for the first principles calculation. Besides the hole-type centers, x-ray irradiation also creates a trapped electron center characterized by the  $g$  factor 1.98. However, no detailed studies are performed for this center.

TSL measurements performed for the same crystals used in EPR show approximately the same composite glow

peaks in YAG and LuAG crystals in the temperature range of 77–280 K. The temperature positions of the peaks correlate with thermal stability of the  $O^-$  STH and  $O^-$ - $Mg^{2+}$  centers suggesting that these peaks mainly originate from thermal destruction of the  $O^-$  centers.

Thermal stability parameters of the traps contributing to TSL (trap depth/ionization energy and frequency parameter) are determined from numerical analysis of corresponding peaks based on the formula of Garlick-Gibson [61]. In particular, the ionization energy of the  $O^-$  STH center is 0.25–0.26 eV. It increases to 0.41–0.45 eV for the  $O^-$ - $Mg^{2+}$  centers.

From an application point of view, knowledge about the presence of intrinsic hole traps in Y and Lu garnets is important as these hole traps participate in the scintillation mechanism. Their impact on scintillation response is, in general, negative as the temporally trapped holes produce delayed recombination at activator (luminescent) ions. They act as competing nonradiative centers, reducing the radioluminescence intensity of rare earth activator ions, such as  $Ce^{3+}$  or  $Pr^{3+}$  [44,51]. On the other hand, in the Ce-doped crystals, the  $O^-$  hole centers may have a positive effect. First, the stored holes at oxygen ions stabilize and dynamically restore the  $Ce^{4+}$  centers, which provides an additional fast recombination pathway in the scintillation mechanism (see Ref. [15], for details). Second, the [ $Mg^{2+}$ -antisite ion] hole traps prevent the antisite defects from participating in electron trapping, thus the efficiency of scintillation at  $Ce^{3+}$  ions could again be increased. This demonstrates that the scintillation performance of Y and Lu garnets can be further optimized by tuning the  $Ce^{3+}/Ce^{4+}$  ratio and  $O^-$  concentrations. Two of these centers can be easily monitored by EPR. Consequently, the gained knowledge regarding the nature of hole centers in garnet scintillators we report in this paper can be used for their further optimization and extended use in practical applications. Furthermore, it will serve as a guide in other oxide scintillators (perovskites, silicates) for their improvement as well.

### ACKNOWLEDGMENTS

The financial support of the Czech Science Foundation Grant No. 17-09933S and the Ministry of Education, Youth and Sports of Czech Republic, projects SAFMAT LO1409 and CZ.02.1.01/0.0/16\_013/0001406 are gratefully acknowledged.

- 
- [1] M. Mosynski, T. Ludziewski, D. Wolski, W. Klamra, and L. O. Norlin, Properties of the YAG:Ce scintillator, *Nucl. Instrum. Methods Phys. Res. A* **345**, 461 (1994).  
 [2] R. Ausrata, P. Schauer, J. Kvapil, and J. Kvapil, A single crystal of YAG-new fast scintillator in SEM, *J. Phys. E: Sci. Instrum.* **11**, 707 (1978).

- [3] D. T. Haven, D. Solodovnikov, M. H. Weber, and K. G. Lynn, Quenched ultraviolet defect emission and excellent scintillation performance on a photodiode from heavily cerium doped yttrium aluminum garnet, *Appl. Phys. Lett.* **101**, 041101 (2012).  
 [4] A. Lempicki, M. H. Randles, D. Wisniewski, M. Balcerzyk, C. Brecher, and A. J. Wojowitz, LuAlO<sub>3</sub>:Ce and other aluminate scintillators, *IEEE Trans. Nucl. Sci.* **42**, 280 (1995).  
 [5] M. Nikl, V. V. Laguta, and A. Vedda, Complex oxide scintillators: Material defects and scintillation performance, *Phys. Status Solidi B* **245**, 1701 (2008).  
 [6] M. Nikl, E. Mihokova, J. A. Mares, A. Vedda, M. Martini, K. Nejezchleb, and K. Blazek, Traps and timing characteristics of LuAG:Ce<sup>3+</sup> scintillator, *Phys. Status Solidi B* **181**, R10 (2000).  
 [7] M. Nikl, A. Yoshikawa, K. Kamada, K. Nejezchleb, C. R. Stanek, J. A. Mares, and K. Blazek, Development of LuAG-based scintillator crystals – A review, *Progr. Cryst. Growth Charact. Mater.* **59**, 47 (2013).  
 [8] Z. Xia and A. Meijerink, Ce<sup>3+</sup>-doped garnet phosphors: Composition modification, luminescence properties and applications, *Chem. Soc. Rev.* **46**, 275 (2017).  
 [9] E. Auffray, A. Fedorov, V. Dormenev, J. Houzvicka, M. Korjik, M. T. Lucchini, V. Mechinsky, and S. Ochesanu, Optical transmission damage of undoped and Ce doped Y<sub>3</sub>Al<sub>5</sub>O<sub>12</sub> scintillation crystals under 24 GeV protons high fluence, *Nucl. Instrum. Methods Phys. Res., Sect. A* **856**, 7 (2017).  
 [10] A. Djebli, F. Boudjada, K. Pauwels, V. Kononets, G. Patton, A. Benaglia, M. Lucchini, F. Moretti, O. Sidletskiy, C. Dujardin, P. Lecoq, F. Auffray, and K. Lebbou, Growth and characterization of Ce-doped YAG and LuAG fibers, *Opt. Mater.* **65**, 66 (2017).  
 [11] Ji. Kvapil, Jo. Kvapil, B. Manek, B. Perner, R. Ausrata, and P. Schauer, Czochralski growth of YAG:Ce in a reducing protective atmosphere, *J. Cryst. Growth* **52**, 542 (1981).  
 [12] Y. Kuwano, K. Suda, N. Ishizawa, and T. Yamada, Crystal growth and properties of (Lu,Y)<sub>3</sub>Al<sub>5</sub>O<sub>12</sub>, *J. Crystal Growth* **260**, 159 (2004).  
 [13] A. G. Petrosyan, K. L. Ovanesyan, R. V. Sargsyan, G. O. Shirinyan, D. Abler, E. Auffray, P. Lecoq, C. Dujardin, and C. Pedrini, Bridgman growth and site occupation in LuAG:Ce scintillator crystals, *J. Crystal Growth* **312**, 3136 (2010).  
 [14] W. Chewpraditkul, L. Swiderski, M. Moszynski, T. Szczesniak, A. Syntfeld-Kazuch, C. Wanarak, and P. Lim-suwan, Scintillation properties of LuAG:Ce, YAG:Ce and LYSO:Ce crystals for gamma-ray detection, *IEEE Trans. Nucl. Sci.* **56**, 3800 (2009).  
 [15] M. Nikl, V. Babin, J. Pejchal, V. V. Laguta, M. Buryi, J. A. Mares, K. Kamada, S. Kurosawa, A. Yoshikawa, D. Panek, T. Parkman, P. Bruza, K. Mann, and M. Muller, The stable Ce<sup>4+</sup> center: A new tool to optimize Ce-doped oxide scintillators, *IEEE Trans. Nucl. Sci.* **63**, 433 (2016).  
 [16] M. Nikl, A. Vedda, M. Fasoli, I. Fontana, V. V. Laguta, E. Mihokova, J. Pejchal, J. Rosa, and K. Nejezchleb, Shallow traps and radiative recombination processes in Lu<sub>3</sub>Al<sub>5</sub>O<sub>12</sub>:Ce single crystal scintillator, *Phys. Rev. B* **76**, 195121 (2007).



- [17] V. V. Laguta and M. Nikl, Electron spin resonance of paramagnetic defects and related charge carrier traps in complex oxide scintillators, *Phys. Status Solidi B* **250**, 254 (2013).
- [18] M. Nikl, J. Pejchal, E. Mihokova, J. A. Mares, H. Ogino, A. Yoshikawa, T. Fukuda, A. Vedda, and C. D'Ambrosio, Antisite defect-free  $\text{Lu}_3(\text{Ga}_x\text{Al}_{1-x})_5\text{O}_{12}:\text{Pr}$  scintillator, *Appl. Phys. Lett.* **88**, 141916 (2006).
- [19] K. Kamada, T. Yanagida, T. Endo, K. Tsutumi, Y. Fujimoto, A. Fukabori, A. Yoshikawa, J. Pejchal, and M. Nikl, Composition engineering in cerium-doped  $(\text{Lu},\text{Gd})_3(\text{Ga},\text{Al})_5\text{O}_{12}$  single-crystal scintillators, *Cryst. Growth Des.* **11**, 4484 (2011).
- [20] Y. Wu, F. Meng, Q. Li, M. Koschan, and Ch. L. Melcher, Role of  $\text{Ce}^{4+}$  in the Scintillation Mechanism of Codoped  $\text{Gd}_3\text{Ga}_3\text{Al}_2\text{O}_{12}:\text{Ce}$ , *Phys. Rev. Appl.* **2**, 044009 (2014).
- [21] M. Yoshino, K. Kamada, Y. Shoji, A. Yamaji, S. Kurosawa, Y. Ohashi, A. Yoshikawa, and V. I. Chani, Effect of Mg co-doping on scintillation properties of  $\text{Ce}:\text{Gd}_3(\text{Ga}, \text{Al})_5\text{O}_{12}$  single crystals with various Ga/Al ratios, *J. Crystal Growth* **468**, 420 (2017).
- [22] J. M. Ogiegłó, A. Katelnikovas, A. Zych, Th. Jüstel, A. Meijerink, and C. R. Ronda, Luminescence and luminescence quenching in  $\text{Gd}_3(\text{Ga},\text{Al})_5\text{O}_{12}$  scintillators doped with  $\text{Ce}^{3+}$ , *J. Phys. Chem. A* **117**, 2479 (2013).
- [23] O. Sidletskiy, V. Kononets, K. Lebbou, S. Neicheva, O. Voloshina, V. Bondar, V. Baumer, K. Belikov, A. Gektin, B. Grinyov, and M.-F. Joubert, Structure and scintillation yield of Ce-doped Al–Ga substituted yttrium garnet, *Mater. Res. Bull.* **47**, 3249 (2012).
- [24] W. Drozdowski, K. Brylew, M. E. Witkowski, A. J. Wojtowicz, P. Solarz, K. Kamada, and A. Yoshikawa, Studies of light yield as a function of temperature and low temperature thermoluminescence of  $\text{Gd}_3\text{Al}_2\text{Ga}_3\text{O}_{12}:\text{Ce}$  scintillator crystals, *Opt. Mater.* **36**, 1665 (2014).
- [25] K. Kamada, Y. Shoji, V. V. Kochurikhin, A. Nagura, S. Okumura, S. Yamamoto, J. Y. Yeom, S. Kurosawa, J. Pejchal, Y. Yokota, Y. Ohashi, M. Nikl, M. Yoshino, and A. Yoshikawa, Large size Czochralski growth and scintillation properties of  $\text{Mg}^{2+}$  Co-doped  $\text{Ce}:\text{Gd}_3\text{Ga}_3\text{Al}_2\text{O}_{12}$ , *IEEE Trans. Nucl. Sci.* **63**, 443 (2016).
- [26] S. K. Yadav, B. P. Uberuaga, M. Nikl, C. Liang, and C. R. Stanek, Band-Gap and Band-Edge Engineering of Multi-component Garnet Scintillators from First Principles, *Phys. Rev. Appl.* **4**, 054012 (2015).
- [27] K. Kamada, S. Kurosawa, P. Prusa, M. Nikl, V. V. Kochurikhin, T. Endo, K. Tsutumi, H. Sato, Y. Yokota, K. Sugiyama, and A. Yoshikawa, Cz grown 2-inch size  $\text{Ce}:\text{Gd}_3(\text{Al},\text{Ga})_5\text{O}_{12}$  single crystal; relationship between Al, Ga site occupancy and scintillation properties, *Opt. Mater.* **36**, 1942 (2014).
- [28] M. Nikl and A. Yoshikawa, Recent R&D trends in inorganic single-crystal scintillator materials for radiation detection, *Adv. Opt. Mater.* **3**, 463 (2015).
- [29] C. R. Stanek, M. R. Levy, K. J. McClellan, B. P. Uberuaga, and R. W. Grimes, Defect identification and compensation in rare earth oxide scintillators, *Nucl. Instrum. Methods Phys. Res. B* **266**, 2657 (2008).
- [30] M. Nikl, E. Mihokova, J. Pejchal, A. Vedda, Y. Zorenko, and K. Nejezchleb, The antisite  $\text{Lu}_{\text{Al}}$  defect-related trap in  $\text{Lu}_3\text{Al}_5\text{O}_{12}:\text{Ce}$  single crystal, *Phys. Status Solidi B* **242**, R119 (2005).
- [31] M. M. Kuklja, Defects in yttrium aluminium perovskite and garnet crystals: Atomistic study, *J. Phys.: Condens. Matter* **12**, 2953 (2000).
- [32] C. Milanese, V. Buscaglia, F. Maglia, and U. Anselmi-Tamburini, Disorder and nonstoichiometry in synthetic garnets  $\text{A}_3\text{B}_5\text{O}_{12}$  (A=Y, Lu–La, B=Al, Fe, Ga). A simulation study, *Chem. Mater.* **16**, 1232 (2004).
- [33] C. R. Stanek, K. J. McClellan, M. R. Levy, C. Milanese, and R. W. Grimes, The effect of intrinsic defects on  $\text{RE}_3\text{Al}_5\text{O}_{12}$  garnet scintillator performance, *Nucl. Instrum. Methods Phys. Res. A* **579**, 27 (2007).
- [34] N. Nikl, Energy transfer phenomena in the luminescence of wide band-gap scintillators, *Phys. Status Solidi A* **202**, 201 (2005).
- [35] V. V. Laguta, M. Nikl, A. Vedda, E. Mihokova, J. Rosa, and K. Blazek, Hole and electron traps in the  $\text{YAlO}_3$  single crystal scintillator, *Phys. Rev. B* **80**, 045114 (2009).
- [36] V. Babin, V. Gorbenko, I. Kondakova, T. Kärner, V. V. Laguta, M. Nikl, S. Zazubovich, and Yu. Zorenko, Time-resolved spectroscopy of exciton states in single crystals and single crystalline films of  $\text{YAlO}_3$  and  $\text{YAlO}_3:\text{Ce}$ , *J. Phys. D: Appl. Phys.* **44**, 315402 (2011).
- [37] Y. Zorenko, V. Gorbenko, T. Voznyak, V. Savchyn, S. Nizhankovskiy, A. Dan'ko, V. Puzikov, V. Laguta, J. A. Mares, M. Nikl, K. Nejezchleb, M. Batentschuk, and A. Winnacker, Luminescent and scintillation properties of  $\text{Lu}_3\text{Al}_5\text{O}_{12}:\text{Sc}$  single crystal and single crystalline films, *Opt. Mater.* **34**, 2080 (2012).
- [38] N. Gautier, M. Gervails, C. Landron, D. Massiot, and J.-P. Coutures, Aluminium–gallium substitution in yttrium garnets investigated by NMR and x-ray absorption, *Phys. Status Solidi A* **165**, 329 (1998).
- [39] E. V. Charnaya, C. Tien, J. J. Lu, R. R. Wu, S. N. Ivanov, and E. N. Khazanov,  $^{27}\text{Al}$  nuclear magnetic resonance studies of the  $\text{Y}_{3-x}\text{Lu}_x\text{Al}_5\text{O}_{12}$  mixed garnets, *J. Phys.: Condens. Matter* **13**, 8775 (2001).
- [40] Our unpublished data.
- [41] K. Mori, Transient colour centres caused by UV light irradiation in yttrium aluminium garnet crystals, *Phys. Status Solidi A* **42**, 375 (1977).
- [42] D. Fagundes-Peters, N. Martynyuk, K. Lunstedt, V. Peters, K. Petermann, G. Huber, S. Basun, V. Laguta, and A. Hofstaetter, High quantum efficiency YbAG-crystals, *J. Lumin.* **125**, 238 (2007).
- [43] C. Hu, S. Liu, M. Fasoli, A. Vedda, M. Nikl, X. Feng, and Y. Pan,  $\text{O}^-$  centers in  $\text{LuAG}:\text{Ce},\text{Mg}$  ceramics, *Phys. Status Solidi RRL* **9**, 245 (2015).
- [44] S. Liu, X. Feng, Z. Zhou, M. Nikl, Y. Shi, and Y. Pan, Effect of  $\text{Mg}^{2+}$  co-doping on the scintillation performance of  $\text{LuAG}:\text{Ce}$  ceramics, *Phys. Status Solidi RRL* **8**, 105 (2014).
- [45] S. Liu, J. A. Mares, X. Feng, A. Vedda, M. Fasoli, Y. Shi, H. Kou, A. Beitlerova, L. Wu, C. D'Ambrosio, Y. Pan, and M. Nikl, Towards bright and fast  $\text{Lu}_3\text{Al}_5\text{O}_{12}:\text{Ce},\text{Mg}$  optical ceramics scintillators, *Adv. Opt. Mater.* **4**, 731 (2016).

- [46] P. Dorenbos, Fundamental limitations in the performance of  $\text{Ce}^{3+}$ ,  $\text{Pr}^{3+}$ , and  $\text{Eu}^{2+}$  activated scintillators, *IEEE Trans. Nucl. Sci.* **57**, 1162 (2010).
- [47] O. F. Schirmer,  $\text{O}^-$  bound small polarons in oxide materials, *J. Phys.: Condens. Matter* **18**, R667 (2006).
- [48] V. V. Laguta, M. Buryi, M. Nikl, J. Rosa, and S. Zazubovich, Hole capture in  $\text{PbWO}_4:\text{Mo},\text{La}(\text{Y})$  scintillator crystals, *Phys. Rev. B* **83**, 094123 (2011).
- [49] V. V. Laguta, M. Buryi, J. Rosa, D. Savchenko, J. Hybler, M. Nikl, S. Zazubovich, T. Karner, C. R. Stanek, and K. J. McClellan, Electron and hole traps in yttrium orthosilicate single crystals: The critical role of Si-unbound oxygen, *Phys. Rev. B* **90**, 064104 (2014).
- [50] D. A. Spassky, V. Nagirnyi, V. V. Mikhailin, A. E. Savon, A. N. Belsky, V. V. Laguta, M. Buryi, E. N. Galashov, V. N. Shlegel, I. S. Voronina, and B. I. Zadneprovski, Trap centers in molybdates, *Opt. Mater.* **35**, 2465 (2013).
- [51] J. Pejchal, M. Buryi, V. Babin, P. Prusa, A. Beitlerova, J. Barta, L. Havlak, K. Kamada, A. Yoshikawa, V. Laguta, and M. Nikl, Luminescence and scintillation properties of Mg-codoped  $\text{LuAG}:\text{Pr}$  single crystals annealed in air, *J. Lumin.* **181**, 277 (2017).
- [52] A. Yoshikawa, M. Nikl, G. Boulon, and T. Fukuda, Challenge and study for developing of novel single crystalline optical materials using micro-pulling-down method, *Opt. Mater.* **30**, 6 (2007).
- [53] L. Rimai and T. Kushida, Paramagnetic resonance of  $\text{Fe}^{3+}$  in yttrium aluminum, lutetium aluminum, and lutetium gallium garnets, *Phys. Rev.* **143**, 160 (1966).
- [54] V. V. Laguta, A. M. Slipenyuk, M. D. Glinchuk, M. Nikl, J. Rosa, A. Vedda, and K. Nejezchleb, Paramagnetic impurity defects in  $\text{LuAG}$  and  $\text{LuAG}:\text{Sc}$  single crystals, *Opt. Mater.* **30**, 79 (2007).
- [55] F. Euler and J. A. Bruce, Oxygen coordinates of compounds with garnet structure, *Acta Crystallogr.* **19**, 971 (1965).
- [56] P. Pyykko, Spectroscopic nuclear quadrupole moments, *Mol. Phys.* **99**, 1617 (2001).
- [57] O. F. Schirmer, K. W. Blazey, and W. Berlinger, ESR and optical absorption of bound-small polarons in  $\text{YAlO}_3$ , *Phys. Rev. B* **11**, 4201 (1975).
- [58] J. T. Devreese, in *Encyclopedia of Applied Physics*, (Wiley-VCH Publishers, Inc., Weinheim, 1996), Vol. 14, pp. 383–409 (arXiv:cond-mat/0004497v2).
- [59] J. Appel, in *Solid State Physics*, edited by F. Seitz, D. Turnbull, H. Ehrenreich (Academic Press, New York, 1968), Vol. 21, pp. 193–391.
- [60] O. F. Schirmer, Holes bound as small polarons to acceptor defects in oxide materials: Why are their thermal ionization energies so high?, *J. Phys.: Condens. Matter* **23**, 334218 (2011).
- [61] S. W. S. Mc Keever, *Thermoluminescence of Solids* (Cambridge University Press, Cambridge, United Kingdom, 1985).